Assessing the Impact of Including Leaflets in the Simulation of TAVI Deployment into a Patient Specific Aortic Root.

Jonathon Bailey[a], Nick Curzen[b], Neil W. Bressloff[c, *]

[a] Computational Engineering and Design Group, Faculty of Engineering and the Environment, The University of Southampton. Address: Building 176 – Room 5017, University of Southampton, Boldrewood campus, Southampton, Hampshire, SO16 7QF, UK. Tel.: +44 07898846960; E-mail: J.Bailey@soton.ac.uk.

[b] Southampton University Hospitals NHS Trust. Address: E Level North Wing, University Hospital Southampton NHS Foundation Trust, Southampton SO16 6YD, UK. Tel.: +44 02380794972, E-mail: Nick.Curzen@uhs.nhs.uk.

[c] Computational Engineering and Design Group, Faculty of Engineering and the Environment, The University of Southampton. Address: Building 176 – Room 5031, University of Southampton, Boldrewood campus, Southampton, Hampshire, SO16 7QF, UK. Tel.: +44 02380 595473; fax: +44 02380 594813; E-mail: N.W.Bressloff@soton.ac.uk.

* Corresponding author.

Word count: 3700

Abstract

Computational simulation of TAVI device deployment presents a significant challenge over and above similar simulations for percutaneous coronary intervention due to the presence of prosthetic leaflets. In light of the complexity of these leaflets, simulations have been performed to assess the effect of including the leaflets in a complete model of a balloon-expandable TAVI device when deployed in a patient-specific aortic root. Using an average model discrepancy metric, the average frame positions (with and without the leaflets) are shown to vary **by 0.236% of the expanded frame diameter (26mm). This relatively small discrepancy leads to the conclusion that for a broad range of replacement valve studies, including new frame configurations and designs, patient-specific assessment of apposition, paravalvular leakage and tissue stress, modelling of the prosthetic leaflets is likely to have a marginal effect on the results.**

Keywords

TAVI, TAVR, leaflets, simulation, deploy and FEA.

Introduction

As life expectancy increases, there are more and more cases of age-related diseases presenting to medical attention (Bonow et al. 2008). Aortic stenosis (AS) is a common age-related heart condition in which there is a thickening and distortion of the valve leaflets together with calcium deposition in the aortic root and valve. This inhibits proper function of the leaflets and can result in a host of further symptoms including angina, embolism, stroke and sudden death (Bertrand et al. 1981; Daneault et al. 2011; Keeley et al. 1998; Smucker et al. 1988; Webb et al. 2009). In a US study of 11,911 patients, aortic stenosis was present in 13.3% of people over 75 years of age (Nkomo et al 2006).

Surgical aortic valve replacement (SAVR) of the calcified valve is the current default treatment for AS. However, surgical intervention is extremely invasive meaning that a large population of frail patients are deemed too high risk for SAVR. Transcatheter aortic valve implantation (TAVI) was developed as a percutaneous alternative to SAVR. A TAVI device was first implanted into a human in 2002 and, since then, more than 50,000 devices have been implanted worldwide (Cribier 2012).

Mortality after TAVI has been associated with severe paravalvular aortic regurgitation (PAR) (Tamburino et al. 2011). PAR occurs when the frame of the TAVI device does not make an effective seal against the internal surface of the aortic root, allowing blood to flow backwards about the valve. PAR is common in patients and has been reported to some degree in as much as 76% of cases. Severe PAR (grade 3 or 4) has been reported in approximately 17% of TAVI patients (Nombela-Franco et al. 2012). Abdel-Wahab et al. (2011) reported that if severe PAR does occur, the incidence of in-hospital mortality is increased from 6.7% to 16.5%. **Balloon angioplasty post deployment, or deploying a second TAVI device into**

the first, has been shown to reduce PAR but can also result in complications including aortic rupture (Hayashida et al. 2012; Kempfert et al. 2013).

Although in some cases PAR can be treated, research is being invested in computational simulation of TAVI device deployment in order to predict and, subsequently, avoid PAR. To date there have been relatively few papers published that describe computational methods for simulating TAVI deployment. Most of the papers neglected to include either the leaflets or the cuff (Capelli et al. 2012; Russ et al. 2013; Tzamtzis et al. 2013; Wang et al. 2012; Wang et al. 2014). Only a single paper included prosthetic leaflets but modelled them using a post deployment mapping technique to align the leaflets with the frame (Auricchio et al. 2014)).

In order for these deployment simulations to be meaningful, the frame position post-deployment must be accurate. The publications above fail to recognise the effect leaflets have on the frames position post deployment. **The leaflets presented in the literature, which are a product of the leaflet mapping technique, fail to capture the actual morphology of the leaflets, something which is visually apparent. Furthermore, the leaflets are represented as surfaces which offer inferior stress calculation within the leaflets when compared to volumised elements.**

So, to date, a complete TAVI deployment simulation does not appear to have been reported that includes an accurate model of TAVI leaflets. This paper describes the techniques required to computationally simulate the deployment of a complete TAVI device by means of balloon inflation, and assesses the necessity of including the leaflets in deployment simulations.

Methodology

The TAVI device modelled herein is based on an Edwards Lifesciences 26mm SAPIEN XT **(The 23mm and 29mm variants of the SAPIEN XT are pictured in Figure 1)**. The model has multiple components: a cobalt chromium alloy frame, a cuff holding the leaflets to the frame, the leaflets themselves and metallic clips restraining the leaflets all of which were designed in Rhinoceros 3D (Robert McNeel & Associates 2014). Explicit finite element analysis was then used to setup and simulate the deployment procedure in ABAQUS CAE/ Explicit V.6-12 (Simulia 2014).

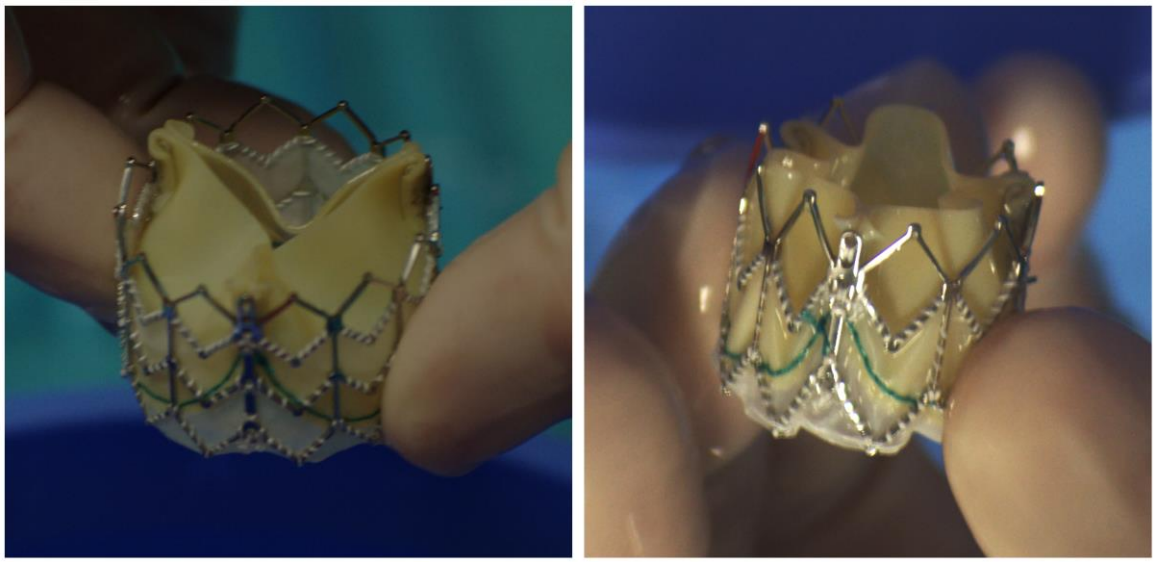

Figure 1. Edwards SAPIEN XT TAVI valves size 29mm (left) and 23mm (right).

Leaflets

The leaflets in a functional position have a complex shape which is difficult to both construct in CAD software and then mesh. As a result, the leaflets were constructed in a planar position and then manipulated into a functional shape using a sequence of geometric operations. As the leaflets are manufactured from bovine pericardium, it can be assumed that the tissue used comprises planar sheets (Mylotte et al. 2012). Conveniently, highly regular meshes **(characterised by non-distorted elements, all of which are of a similar size)** can be generated in the planar leaflet model that are resistant to excessive distortion, even in areas of the leaflets that are prone to high deformation when deployed. The highly regular mesh used to model the leaflets contained 135,536 elements and four nodes across the thickness of the leaflet. **The leaflets are known to be manufactured from bovine pericardium, which is an orthotropic material. The in-plane material properties are uniform and the out-of-plane stiffness is significantly less. In this study, the material properties are assumed to be isotropic, and adopt the stiffer, in-plane setup.** The material properties were assumed to be hyperelastic and employed the Ogden model wherein the strain energy function is

$$U = \sum_{i=1}^{N} \frac{2\mu_i}{\alpha_i^2}\left(\bar{\lambda}_1^{\alpha i} + \bar{\lambda}_2^{\alpha i} + \bar{\lambda}_3^{\alpha i} - 3\right) + \sum_{i=1}^{N} \frac{1}{D_i}(J^{el} - 1)^{2i} \quad (1)$$

$\lambda_1^{\alpha i}$ are the deviatoric principal stretches, $\bar{\lambda_i} = J^{-\frac{1}{3}}\lambda_i$, λ_i are the principal stretches, **N is the strain energy potential order, in this case 1**, and μ_i, α_i, and D_i are temperature-dependent material properties. In this study, $\mu_i = 0.1591$, $\alpha_i = 10.89$, **$D_1 = 0$ (thus inducing Abaqus to assign a computed default between 6.667-16.667)** and the density, $\rho = 1.1$ g/cm^3 (Lin et al. 2013). The leaflet thickness was 0.3mm and further geometry parameters are defined in Figure 2(B). Only one of the leaflets was modelled and the final shape was duplicated in the final assembly.

The model comprised 12 surfaces (Figure 2), constrained in six degrees of freedom, as well as the planar leaflet and a pair of clips described in the appendix. The surfaces, clips and node

groups on the leaflet were translated in order to manipulate the leaflet into an appropriate final position. When contact between surfaces was defined, the normal contact was ‘hard’ and the tangential behaviour was frictionless. **The leaflet has a plane of symmetry which is shown in Figure 2(B). If the leaflet was to be bisected along the symmetry plane, a group of nodes would be revealed; these nodes are constrained to remain within the symmetry plane, in order to ensure symmetry.**

The five steps of the leaflet manipulation simulation are as follows.

Step 1: Each leaflet was setup to span a 120 degree segment of the valve orifice. The interface between the leaflet being manipulated and its theoretical neighbouring leaflets was represented by surfaces S3 and S4. In this step the leaflet was manipulated to lie within its orifice segment. This was achieved by translating strategic nodes in the leaflet wings (highlighted red in Figure 2(B)). The translation resulted in the leaflet wings being flush with S3 and S4 (Figure 2(D)). This step was modelled as a 0.04s process.

Step 2: During the first step there were no contact definitions defined between the leaflet and the clips (labelled in Figure 2(E)), so as to avoid volumetric intersections. During Step 2, the contact definitions were instated. The clips were then translated in a normal direction to the surfaces S3 and S4, until contact was made with the leaflet, over a time period of 0.02s. Figure 2(E-F) depicts the model with the clips in the original position and final position.

Step 3: The leaflet wings were then wrapped about the clips. This was achieved by systematically translating planar surfaces towards the clips. This is shown in Figure 2(F-G), although only half the system is shown for clarity and it is a symmetrical process. The order in which the surfaces translated was Sa, Sb, Sc and finally Sd (the surfaces are labelled in Figure 2(E)). Each translation lasted 0.015s, resulting in a complete step time of 0.06s.

Step 4: S1 is a cylindrical surface that represents the internal surface of the TAVI frame. The radius of S1 was reduced to 12.6mm by means of a boundary condition (BC) using a cylindrical datum system over a time period of 0.02s. S1 was used to ensure that a volumetric intersection between the leaflet and the frame could not occur. The positions of the surfaces after this step are shown in Figure 2(H).

Step 5: The final step involved pulling the lower edge of the leaflet to the frame; in reality this edge is stitched to a cuff attached to the frame. This was achieved by displacing S2 radially to a radius of 12.6mm, again by means of a BC using a cylindrical datum system. The contact definition between S2 and the leaflet was only implemented along the lower edge. This step was modelled as a 0.03 second process with the final position shown in Figure 2(I).

The final geometry is shown in Figure 2(J-L).

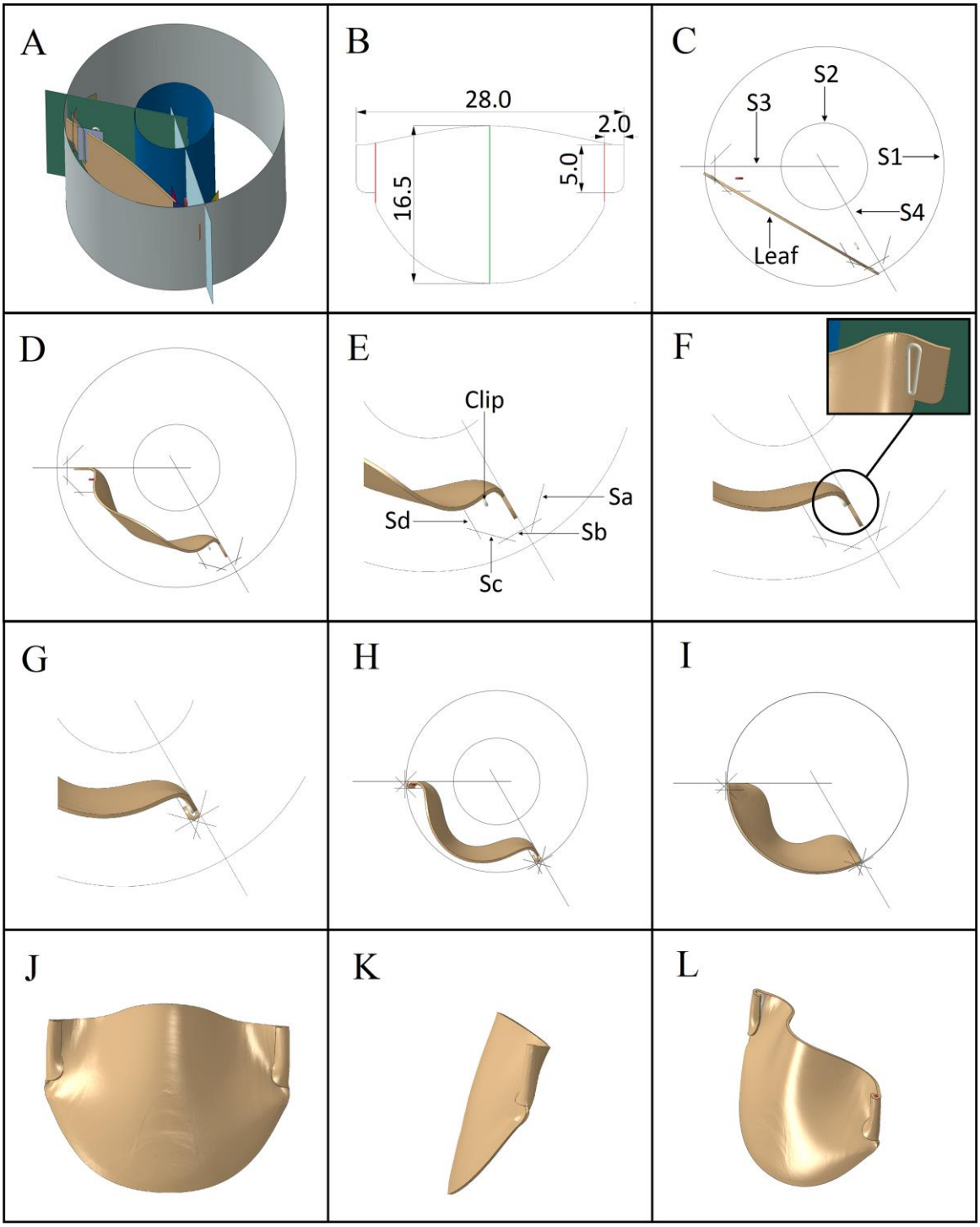

Figure 2, A: Isometric view of the leaflet manipulation system, B: Leaflet geometry the units of which are millimetres, nodes sets X and Y are highlighted in red, a plane of symmetry is highlighted in green, C-I: Depicting the manipulation of the leaflets, J: final geometry rear view, K: final geometry side view, L: final geometry isometric view.

Triple Leaflet Model

In order to check that the leaflet geometry was correct, a second model was developed that tested the ability of the leaflets to close together in a realistic manner. An orphan mesh of the leaflet and its clips was created from the leaflet geometry manipulation simulation. The orphan meshes were duplicated before being repositioned to create a triplet of leaflets (Figure 3(A)). The lower edge of the leaflets which, in reality, are stitched to the frame and the cuff, were constrained in all dimensions, as were all six of the clips. The contact definition employed a penalty friction model with 'hard' normal behaviour and a coefficient of friction equal to 0.2 for the tangential behaviour.

A pressure of 13kPa was applied to the top side of the leaflets to represent the pressure experienced during the cardiac cycle. Contact definitions were applied between all the components and self-contact was applied to the leaflets. The results are shown in Figure 3.

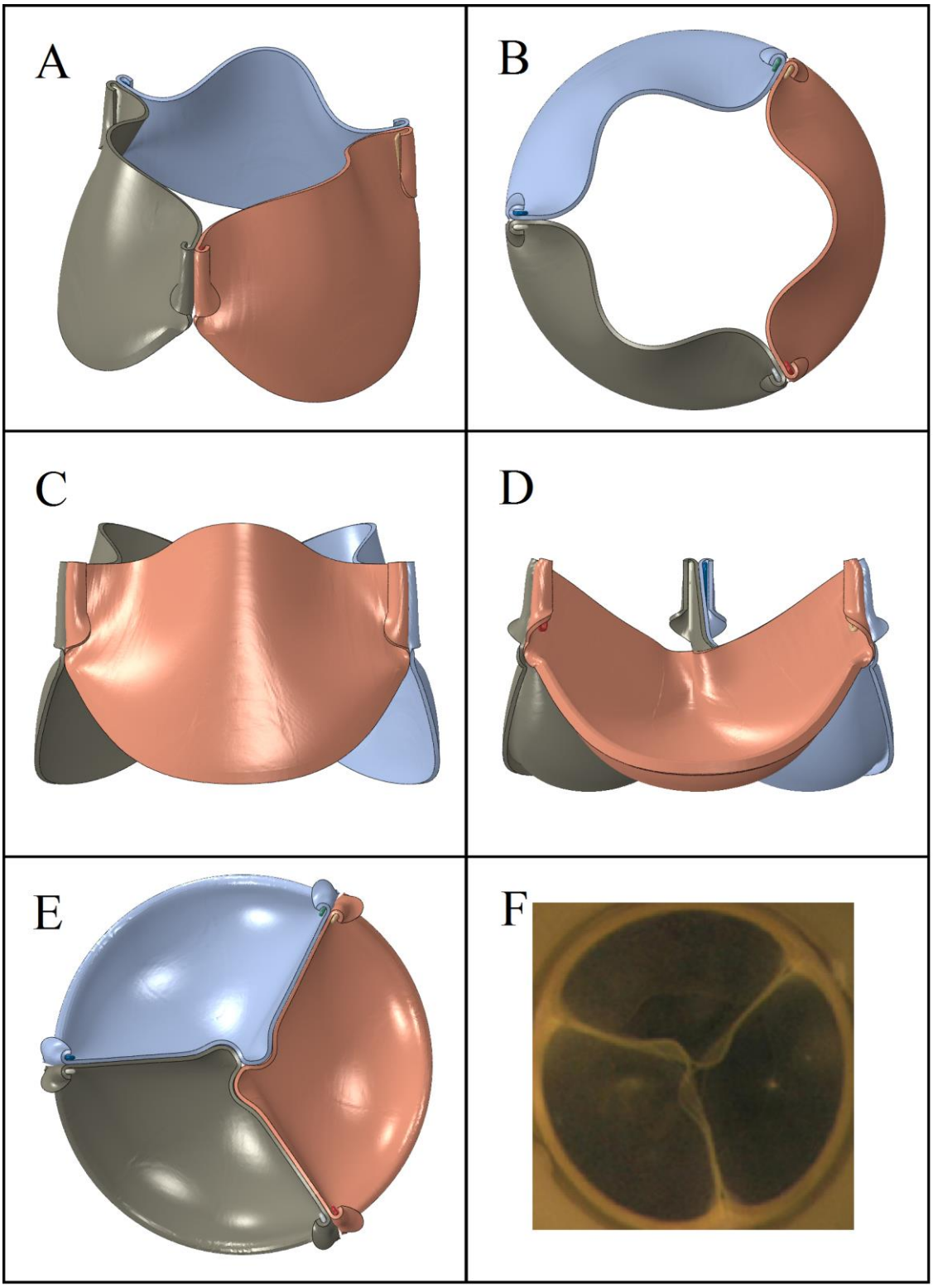

Figure 3. The triple leaflet model in A: open isometric view, B: open top view, C: open side view, D: closed side view, E: closed top view, F: closed top view of an experimental valve.

The simulation showed that the leaflets successfully closed (Figure 3(D-E)) and exhibited a twisting motion in the centre of the leaflets.

Full Model

A complete TAVI device (based on the SAPIEN XT) was constructed from the leaflets described above, and a frame, cuff and clips as described in the appendix. Constraints were used to secure each component in place. Tie constraints were used to attach the cuff to the frame and the leaflets to the cuff. The clips were constrained to the frame with a coupling constraint. Similarly, nodes in the leaflet wings were also constrained to the same control points by means of a coupling constraint.

The complete model was simulated undergoing balloon deployment into a patient specific aortic root model. **A complete aortic root, including native leaflets, was extracted from multi-slice computer tomography (MSCT) data taken from a sixty year old female patient (for further details on the aortic root model, see the appendix). The aortic annulus was oval in shape, with a superior diameter of 28mm and an inferior diameter of 14mm. The material properties assigned to the aortic root, and the native aortic leaflets are summarised in Table 1 (Azadani et al. 2012; Mohammadi et al. 2009).**

Table 1: Material properties of the aortic root wall and native aortic leaflets.		
	Aortic root wall	Native aortic leaflets
Elastic Modulus	2MPa	3.3MPa
Poisson's Ratio	0.45	0.3
Mass Density	$1.1x10^{-9}$	$1.1x10^{-9}$
Rayleigh Damping Factor Alpha Coefficient	2000	2000

In order to assess the impact the leaflets have on the frame position post deployment, the TAVI device components were systematically removed and the simulation repeated. The components present in the TAVI device for each simulation is summarised in **Error! Reference source not found.**.

Table 2. Components included in each simulation.				
Simulation\Component	Frame	Cuff	Clips	Leaflets
Simulation_1	Included	Included	Included	Included
Simulation_2	Included	Included	Included	Excluded
Simulation_3	Included	Included	Excluded	Excluded

Contact definitions ('hard' and frictionless) were defined between pairs of components as presented in Table 3.

Table 3. Contact pairs throughout the deployment simulation.				
Contact pair\step	Step 1	Step 2	Step3	Step 4
Balloon – Balloon	Active	Active	Active	Active
Balloon – Wire	Active	Active	Active	Active
Balloon – Frame	Active	Active	Active	Active
Balloon – Native Leaflets		Active	Active	Active
Balloon – Aortic Root	Active	Active	Active	Active
TAVI Leaflets – TAVI Leaflets	Active	Active	Active	Active
Frame – Frame	Active	Active	Active	Active
Frame – TAVI Leaflets	Active	Active	Active	Active
Native Leaflet – Native Leaflet	Active	Active	Active	Active
Aortic Root – Frame		Active	Active	Active
Aortic Root – Native Leaflet	Active	Active	Active	Active
Crimping Surface - Frame	Active			
Frame – Native Leaflets		Active	Active	Active

Crimping was achieved using an additional cylindrical surface (visible in Figure 4(A)) that was concentric with the frame and a displacement boundary condition was used to radially contract this surface in order to crimp the device.

It was found that 300kPa was a sufficient pressure to inflate the balloon and deploy the device. While higher pressure is used in reality, this lower pressure requires fewer time increments to compute, therefore reducing computational time.

Step 1: In the first step the TAVI device was crimped by means of the cylindrical surface (Figure 4(A-C)). Displacement boundary conditions reduced the diameter of the cylinders to 10mm, thus reducing the diameter of the frame to 10mm at its widest point. Simultaneously, a 300kPa pressure was applied to the underside of the native aortic leaflets in order to open the native valve. As the valve was modelled in the closed position, it must be opened in order to avoid volumetric intersection with the TAVI device (Figure 4(D-E)). This step was modelled over a 0.03s time step.

Step 2: The contact definition between the crimping surface and the frame was removed, and the frame elastically recoiled. The contact definitions between the native leaflets and the TAVI device frame and balloon were implemented, and the pressure applied to the leaflets was deactivated. The native aortic leaflets also recoiled during this step (0.01s) as shown in Figure 4(F-G).

Step 3: An internal pressure was applied to the balloon of magnitude 300kPa over a time period of 0.1s which fully inflated the balloon. This is shown in Figure 4(G-I).

Step 4: The internal pressure of the balloon was decreased with a smooth step over a time period of 0.02s. The balloon returned to its original position through elastic recoil and, furthermore, the TAVI frame recoiled slightly and the leaflets adopted a natural open position. This is shown in Figure 4(I-J).

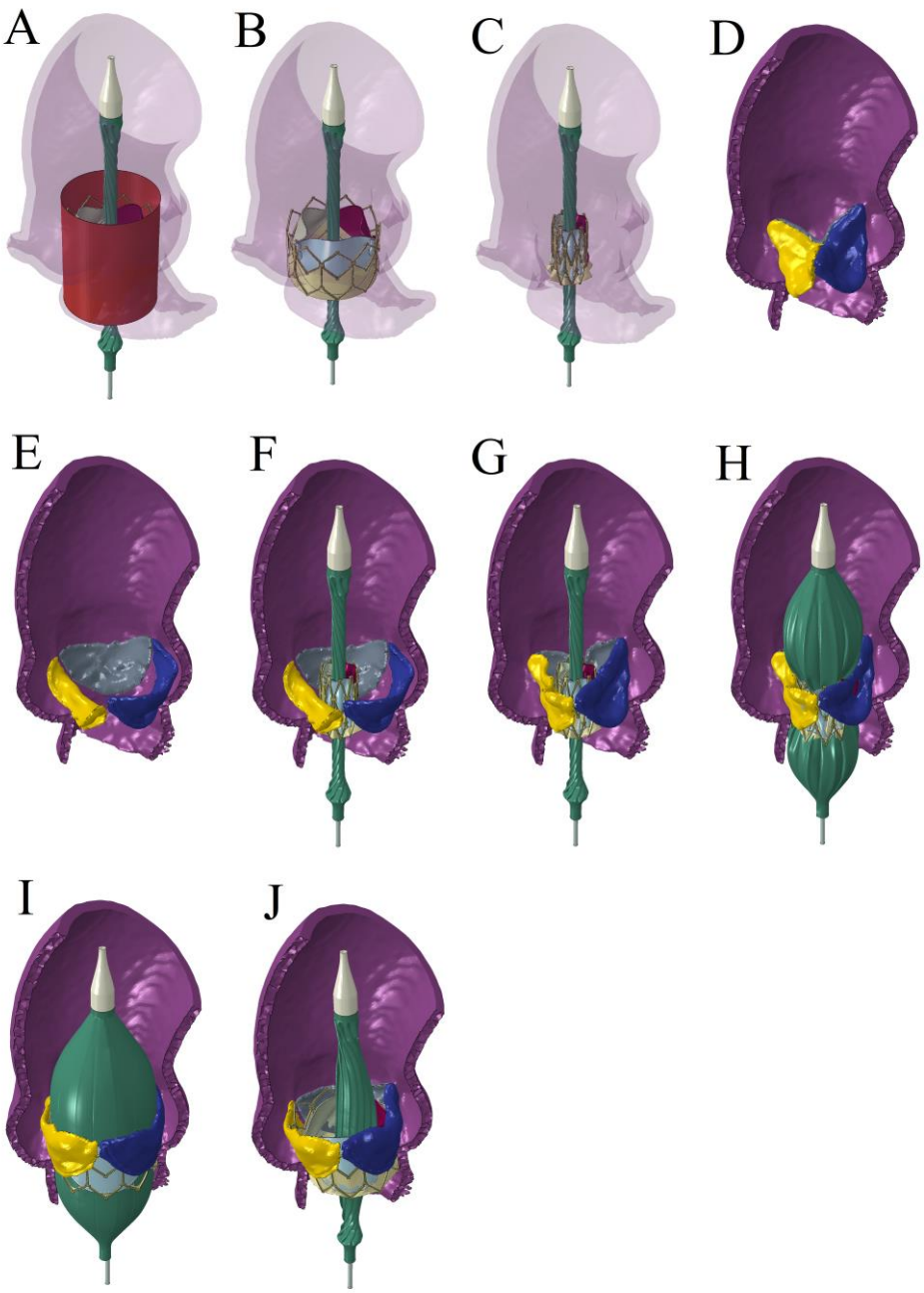

Figure 4. Full device simulation. A-C: The full TAVI device being crimped about the balloon with the aortic root wall (ghosted) and the crimping surface (A only) present. D, E: The native aortic root leaflets opening under a pressure load with the aortic root wall (section removed). F, G: The native leaflets and TAVI devices relaxing during step 2, with the aortic root wall (section removed). G-J: The delivery system deploying the full TAVI device into the aortic root model (section removed from the aortic root wall), before relaxing.

All simulations comprised approximately two million elements and were run across sixteen domains on dual 2.4GHz intel Xeon E5-4640 CPUs in 131 hours.

Results

To quantify discrepancy in frame position, the average nodal position of each frame was calculated and then compared. The average nodal position discrepancies (ANPD) are shown in Table 4.

Table 4. The average nodal position discrepancies between the three simulations.

	Simulation_1	Simulation_2	Simulation_3
Simulation_1	NA	0.0613mm	0.0343mm
Simulation_2	0.0613mm	NA	0.0956mm
Simulation_3	0.0343mm	0.0956mm	NA

Discussion and Limitations

When simulating the deployment of a TAVI device, it is important to gauge and understand the impact of model fidelity. Such verification extends to the value of including the prosthetic leaflets when deploying a device into a patient specific aortic root. Other recent attempts at modelling TAVI device deployment have neglected the leaflets or employed approximate models for them (Auricchio et al. 2014; Capelli et al. 2012; Russ et al. 2013; Tzamtzis et al. 2013; Wang et al. 2012; Wang et al. 2014). Most notably, Auricchio et al. (2014), successfully simulated a TAVI frame deployment into an aortic root and then developed a leaflet model within the frame in its post-procedural position. However, the impact of the

leaflets on the deployment simulation has not been addressed. In contrast, this article describes a successful simulation of a complete TAVI device and studies the impact of including the leaflets.

Figure 5 graphically shows the three frames from each simulation. The frames from Simulation_1 and Simulation_2 are visually very similar and have an average discrepancy, ANPD=0.0613mm, equivalent to **0.236% of the frame diameter (26mm)**. This demonstrates that the inclusion of the leaflets for the deployment simulation has a minimal effect on the post-deployment position of the frame.

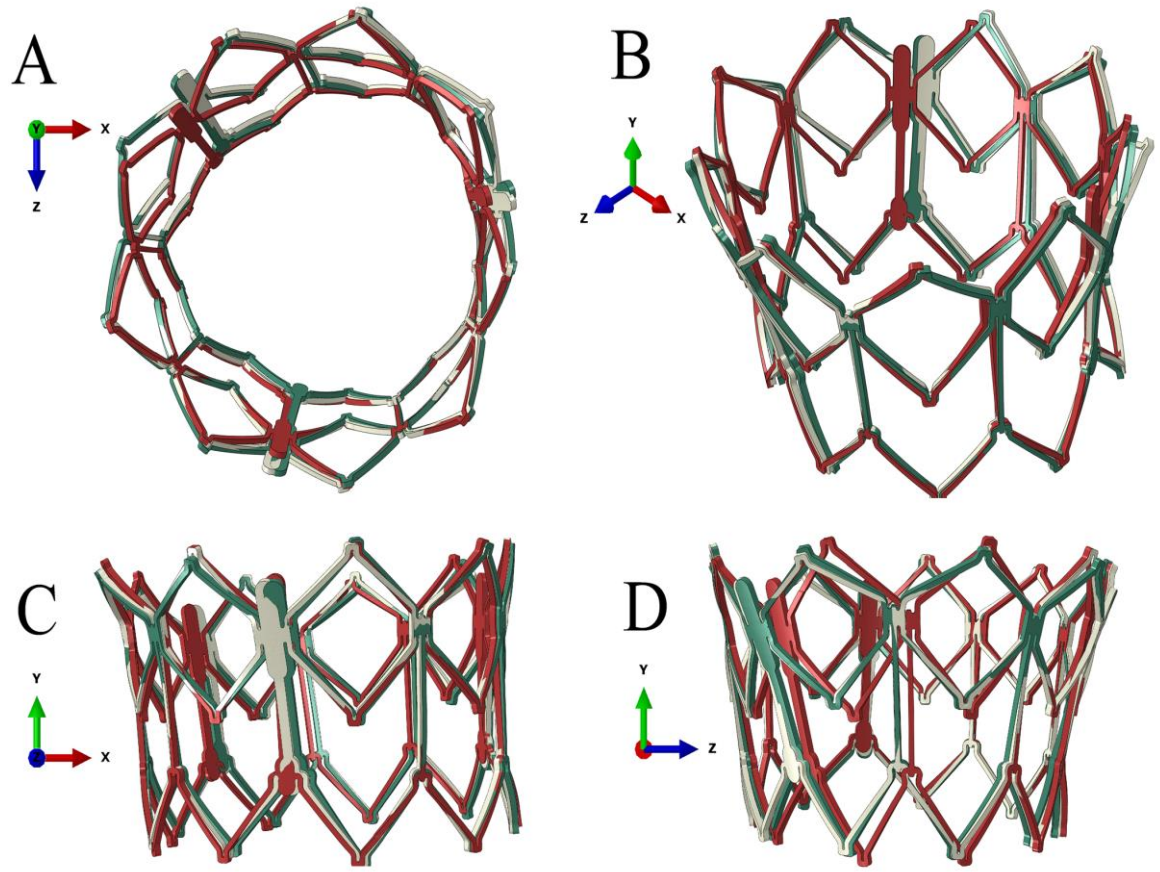

Figure 5. The post-deployment frame position for Simulation_1 (green), Simulation_2 (white) and Simulation_3 (red).

Comparing Simulation_2 with Simulation_3 (ANPD=0.0956mm), it is clear that a larger discrepancy is associated with the clips. This resulted from the constraint applied to the clips to construct the model. Coupling constraints were applied to the clips, which are completely rigid. However, in reality, the clips would be stitched to the frame resulting in a more flexible structure.

The ANPD between Simulation_1 and Simulation_3 is 0.0343mm. This is the smallest discrepancy between the three models, despite the two models varying the greatest.

It was found that the leaflets and cuff can become unstable if severely distorted. As a result, the device was crimped to 10mm in diameter, as opposed to a more realistic diameter of 6mm. A TAVI device represented by the frame alone however, can be crimped to 6mm. Thus, if the application of a simulated TAVI device requires it to be crimped to a more realistic deployment diameter, it may not be possible to include the leaflets, due to the very large distortions that are likely to occur.

Conclusions

A full TAVI model deployment simulation has been described including a previously unreported leaflet manipulation technique that was integral to the simulation. The simulations have shown that the leaflets do not significantly affect the post-deployment position of the frame (average nodal position discrepancy of 0.0613mm, **equivalent to 0.236% of the frames diameter). This relatively small discrepancy leads to the conclusion that for a broad range of replacement valve studies including new frame configurations and designs, patient-specific assessment of apposition, paravalvular leakage and tissue stress, modelling of the prosthetic leaflets is likely to have a marginal effect on results.** The clips were included to constrain the ends of the leaflets, and result in an average nodal position discrepancy of 0.0956mm. This was most likely due to the rigid boundary conditions applied to them.

Acknowledgements

This project was partially funded by Medtronic and the authors of this paper would like to thank Medtronic for the support offered which ultimately allowed the project to be completed.

References

Abdel-Wahab M, Zahn R, Horack M, Gerckens U, Schuler G, Sievert H, Eggebrecht H, Senges J, Richardt G. 2011. Aortic Regurgitation After Transcatheter Aortic Valve Implantation: Incidence and Early Outcome. Results from the German Transcatheter Aortic Valve Interventions Registry. Heart. 97:899-906.

Auricchio F, Conti M, Morganti S, Reali A. 2014. Simulation of Transcatheter Aortic Valve Implantation: a Patient-Specific Finite Element Approach. Comput Methods Biomech Biomed Engin. 1712: 1347-1357.

Azadani A, Chitsaz S, Peter M, Jaussaud N, Leung J, Tsinman T, Ge L, Tseng E. 2012. Comparison of Mechanical Properties of Human Ascending Aorta and Aortic Sinuses. Ann Thorac Surg. 93:87-94.

Bertrand M E, LaBlanche J M, Tilmant P Y, Thieuleux F P, Delforge M R, Carre A G. 1981. Coronary Sinus Blood Flow at Rest and During Isometric Exercise in Patients with Aortic Valve Disease. Mechanism of Angina Pectoris in Presence of Normal Coronary Arteries. Am J Cardiol 47: 199-205.

Bonow R O, Carabello B A, Chatterjee K, de Leon A C, Faxon D P, Freed M D, Gaasch W H, Lytle B W, Nishimura R A, O'Gara P T, et al. 2008. Focused Update Incorporated into the

ACC/AHA 2006 Guidelines for the Management of Patients with Valvular Heart Disease. Circulation 118: 523-661.

Capelli C, Bosi G M, Cerri E, Nordmeyer J, Odenwald T, Bonhoeffer P, Migliavacca F, Taylor A M, Schievano S. 2012. Patient-Specific Simulations of Transcatheter Aortic Valve Stent Implantation. MBEC. 50: 183-192.

Cribier A. 2012. Development of Transcatheter Aortic Valve Implantation (TAVI): A 20-Year Odyssey. Arch Cardiovasc Dis. 105: 146-152.

Daneault B, Kirtane A J, Kodali S K, Williams M R, Genereux P, Reiss G R, Smith C R, Moses J W, Leon M B. 2011. Stroke Associated With Surgical and Transcatheter Treatment of Aortic Stenosis: A Comprehensive Review. J Am Coll Cardiol. 58(21): 2143-2150.

Hayashida K, Lefèvre T, Chevalier B, Hovasse T, Romano M, Garot P, Bouvier E, Farge A, Donzeau-Gouge P, Cormier B, Morice M C. 2012. Impact of Post-Procedural Aortic Regurgitation on Mortality After Transcatheter Aortic Valve Implantation. JACC. 5: 1247-1256.

Keeley E C, Grines C L. 1998. Scraping of Aortic Debris by Coronary Guiding Catheters: a Prospective Evaluation of 1,000 Cases. J Am Coll Cardiol. 32(7): 1861-1865.

Kempfert J, Girrbach F, Haensig M, Subramanian S, Holzhey D, Mohr F. 2013. Transapical Aortic Valve-in-Valve-in-Valve Implantation as a Procedural Rescue Option. Ann Thorac Surg. 95:325-8.

Lin S, Akula P, Gu L. 2013. Mechanical Performance of Bovine Pericardial Bioprosthetic Valves. J Med Devices. 7: 926-926.

Mohammadi H, Bahramian F, Wan W. 2009. Advanced Modeling Strategy for the Analysis of Heart Valve Leaflet Tissue Mechanics Using High-order Finite Element Method. Med Eng and Phys. 31: 1110-1117.

Mylotte D, Martucci G, Piazza N. 2012. Patient Selection for Transcatheter Aortic Valve Implantation: An Interventional Cardiology Perspective. Ann Thorac Surg 1(2): 206-215

Nkomo V T, Gardin J M, Skelton T N, Gottdiener J S, Scott C G, Enriquez-Sarano M. 2006. Burden of Valvular Heart Diseases: a Population-Based Study. Lancet. 368(9540): 1005-1011.

Nombela-Franco L, Rodés-Cabau J, DeLarochellière R, Larose E, Doyle D, Villeneuve J, Bergeron S, Bernier M, Amat-Santos I J, Mok M, et al. 2012. Predictive Factors, Efficacy, and Safety of Balloon Post-Dilation After Transcatheter Aortic Valve Implantation With a Balloon-Expandable Valve. JACC. 5(5): 499-512.

Robert McNeel & Associates. 2014. Rhinoceros3D [DVD]. Version 5. USA.

Russ C, Hopf R, Hirsch S, Sundermann S, Falk V, Szekely G, Gessat M. 2013. Simulation of Transcatheter Aortic Valve Implantation Under Consideration of Leaflet Calcification. Paper presented at: IEEE EMBS. Osaka, Japan.

Simpleware Ltd. 2014. ScanIP: 3D Image Visulisation and Processing Software [DVD]. Version 6. United Kingdom.

Simulia. 2014. Abaqus/Explicit: Complete solutions for realistic simulation [DVD]. Version 6.12. Dassault Systems France.

Smucker M L, Tedesco C L, Manning S B, Owen R M, Feldman M D. 1988. Demonstration of an Imbalance Between Coronary Perfusion and Excessive Load as a Mechanism of Ischemia During Stress in Patients with Aortic Stenosis. Circulation. 78(3): 573-582.

Smuts A N, Blaine D C, Scheffer C, Weich H, Doubell A F, Dellimore K H. 2011. Application of Finite Element Analysis to the Design of Tissue Leaflets for a Percutaneous Aortic Valve. J Mech Behav Biomed Mater. 4(1): 85-98.

Tamburino C, Capodanno D, Ramondo A, Petronio A S, Ettori F, Santoro G, Klugmann S, Bedogni F, Maisano F, Marzocchi A, et al. 2011. Incidence and Predictors of Early and Late Mortality After Transcatheter Aortic Valve Implantation in 663 Patients with Severe Aortic Stenosis. Circulation 123(3): 299-308.

Tzamtzis S, Viquerat J, Yap J, Mullen M J, Burriesci G. 2013. Numerical Analysis of the Radial Force Produced by the Medtronic-CoreValve and Edwards-SAPIEN After Transcatheter Aortic Valve Implantation (TAVI). Med Eng Phys. 35(1): 125-130.

Wang Q, Kodali S, Primiano C, Sun W. 2014. Simulations of transcatheter aortic valve implantation: implications for aortic root rupture. Biomech Model Mechanobiol: 14(1):29-38.

Wang Q, Sirois E, Sun W. 2012. Patient-Specific Modeling of Biomechanical Interaction in Transcatheter Aortic Valve Deployment. J Biomech. 45(11): 1965-1971.

Webb J G, Altwegg L, Boone R H, Cheung A, Ye J, Lichtenstein S, Lee M, Masson J B, Thompson C, Moss R et al. 2009. Transcatheter Aortic Valve Implantation: Impact on Clinical and Valve-Related Outcomes. Circulation. 119(23): 3009-3016.

6. Appendix

Clips

One of the key challenges in this model concerns the method used to connect individual parts together (without using stiches). With respect to the wings of the leaflets, there is a feature visible in Figure 1 that appears to be a clip in the upper corner of the leaflets. The precise nature of this feature is unclear but in this work it is assumed to be a small metallic clip and a pair of clips are assumed to hold adjacent leaflets together. Each clip has a circular cross section of 0.28mm diameter and is wrapped into the shape of a caribena that is 4.5 mm long and 1.12mm in width at the widest point. Each clip was meshed with approximately 10,000 tetrahedral elements. The material properties used to model the clips are tabulated in Table 5.

Table 5. Material properties of each component.

	Cuff (based on polyethylene terephthalate)	Frame and clips (cobalt chromoly MP35N)	Balloon
Elastic modulus	500MPa	232GPa	900MPa
Yield stress	NA	739MPa	NA
Poisson's ratio	0.3	0.3	0.3
Density	1.38g/cm^3	8.4g/cm^3	1.1g/cm^3

Cuff

The cuff is a plastic film that fills the lower cells of the frame to prevent PAR. In reality, the lower edges of the leaflets are stitched to the frame and to the cuff. The geometry of the cuff is controlled entirely by the geometry of the frame as it spans the lower cells as shown in

Figure 6. **The cuff is a thin piece of material, and its ability to withstand bending is negligible. In order to incorporate this into the simulation, the cuff was meshed with membrane elements, totalling 413,207 elements. Assigning material properties to the cuff is difficult as the mechanical properties will vary from the base material (polyethylene terephthalate) as it is so thin. No experimental analysis, or material properties have been suggested for the cuff in the literature. As a result, the cuff thickness was assumed to be 0.01mm, and the elastic modulus was calibrated until the cuff behaved in a realistic manner. Realistic behaviour was considered as stiff enough to constrain the lower edge of the leaflet, while malleable enough to still allow the frame to be crimped. An elastic modulus of 500MPa was found to be sufficient (further material properties can be found in Table 5, which are based on polyethylene terephthalate).**

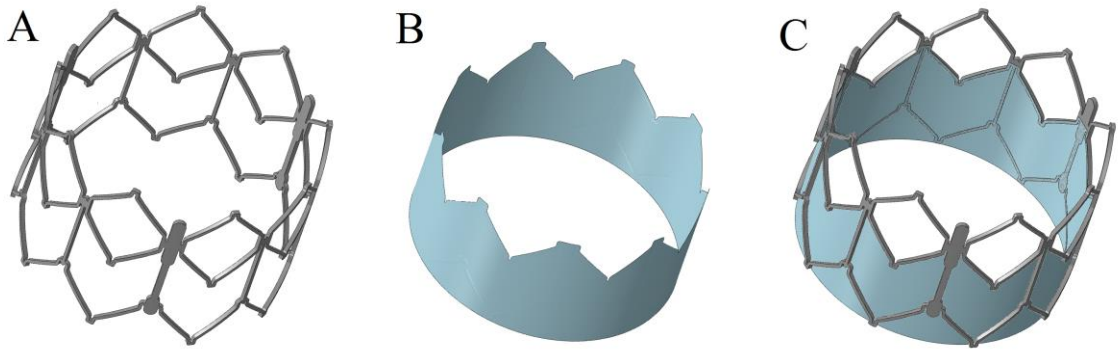

Figure 6. The frame (A), cuff (B) andframe and cuff combined (C).

Frame

The leaflets and cuff are assembled within the metallic frame of the TAVI device. The frame is based on the Edwards Lifesciences SAPIEN XT 26mm TAVI device, and is shown in Figure 6. The frame struts have a rectangular cross section of 0.3mm by 0.4mm and it is manufactured from Co-Cr MP35N, the material properties of which are presented Table 5. A mesh refinement study was performed and concluded that a target element size of 0.08mm has an appropriate level of accuracy, and results in a mesh of 168, linear hexahedral elements.

Balloon

The SAPIEN XT is a balloon expandable device. The balloon model developed here was based on the Edwards Lifesciences NovaFlex+ delivery system. A geometric model of the NovaFlex+ profile was based on a photograph of known scale, from which the model profile was calibrated as shown in Figure 7. The values of the geometric parameters are listed in **Error! Reference source not found.**. **The material thickness of the NovaFlex+ balloon was found to be 0.07mm through measurement of an actual device.** The profile was revolved about the balloon axis to create the balloon surface.

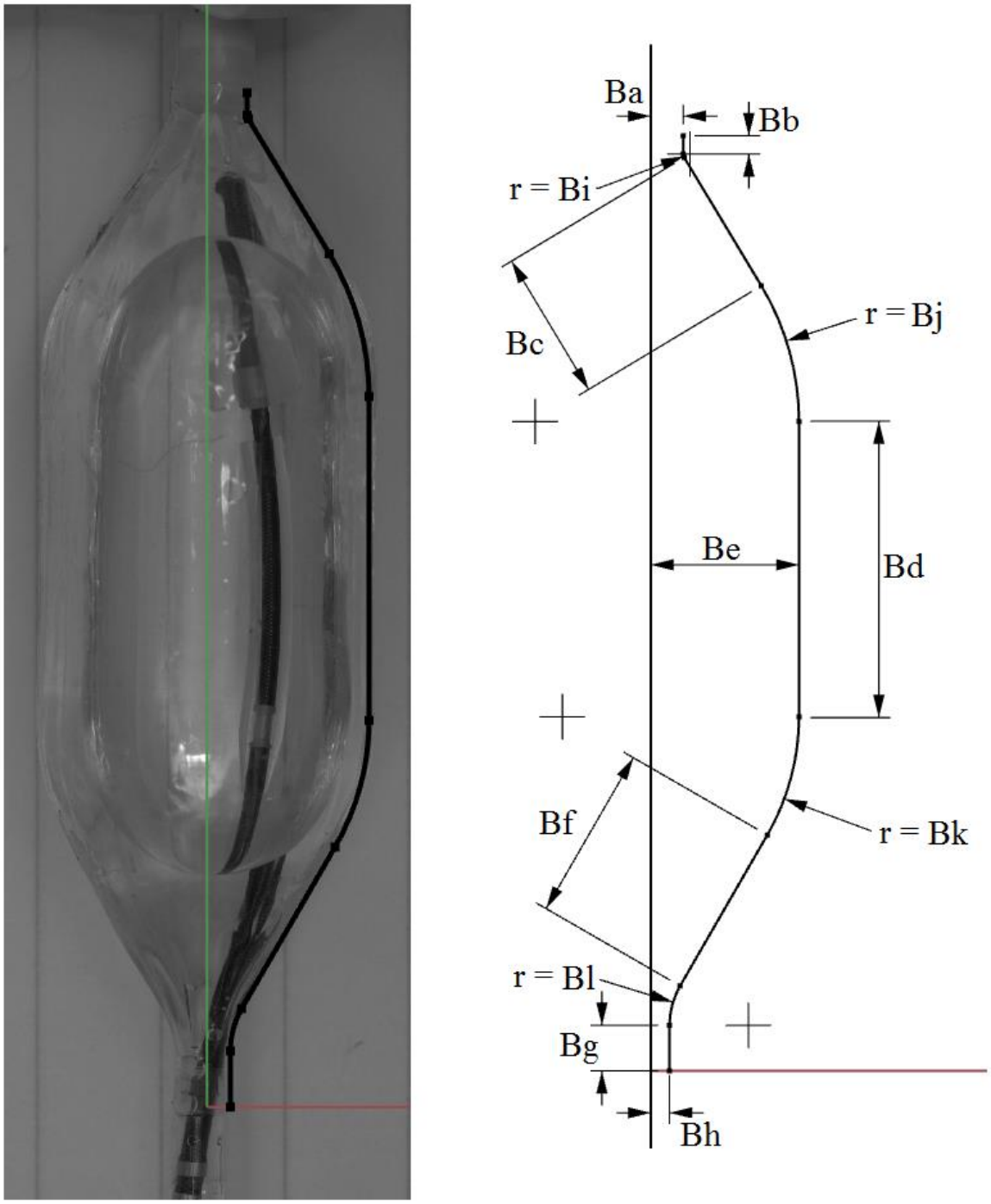

Figure 7. The NovaFlex+ delivery system with the outline of the geometric model overlay (left), the geometric model defined (right).

Table 6. Balloon model geometric coefficients.	
Ba	2.85mm
Bb	1.60mm
Bc	13.13mm
Bd	25.90mm
Be	13.00mm
Bf	15.29mm
Bg	4.00mm
Bh	1.65mm
Bi	0.59mm
Bj	23.13mm
Bk	20.75mm
Bl	6.91mm

The balloon model was setup from an initial inflated state, such that a preliminary simulation was required to deflate and wrap the balloon. The balloon was meshed with a combination of triangular and quadrilateral shell elements, numbering 428,262 and 368,114, respectively. **A NovaFlex+ delivery system was obtained, from which the wall thickness was measured as 0.07mm. The lowest elastic modulus was used capable of expanding a TAVI frame without over expanding or stretching the balloon was found through computational analysis, and subsequently used throughout the simulations. This minimises the energy required to deploy the balloon, which increases simulation stability.** The material properties used to represent the balloon are summarised in Table 5. Preliminary boundary

conditions were applied to the lower edge of the balloon which was constrained to a plane normal to the axis of the balloon. Further tie constraints were used to attach the upper edge of the balloon, and the wire to the cone (the wire and cone are visible in Figure 8(B)). Two node sets were used to apply loads to the balloon: ‘A’ and ‘B’, which are depicted in Figure 8(A). The simulation contact definitions were ‘hard’ normal contact and frictionless tangential behaviour.

The simulation had two distinct steps. In the first step, two loads were applied, the first to set ‘A’ of magnitude 0.04N radially inwards. The second was applied to set ‘B’ with a magnitude of 0.02N radially outwards. This resulted in the cross section of the balloon folding from a circle, to an eight armed star shape. This step is shown in Figure 8(C-F).

In the second step, the node set ‘A’ was constrained in all dimensions, node set ‘B’ had a load of 0.05N applied tangentially about the axis of the balloon. The coordinate system recalculated the direction of the load every increment to retain its tangential orientation to the balloon axis. This is graphically shown in Figure 8(F-I).

The magnitude of load required to fold the balloon was determined through computational experiment.

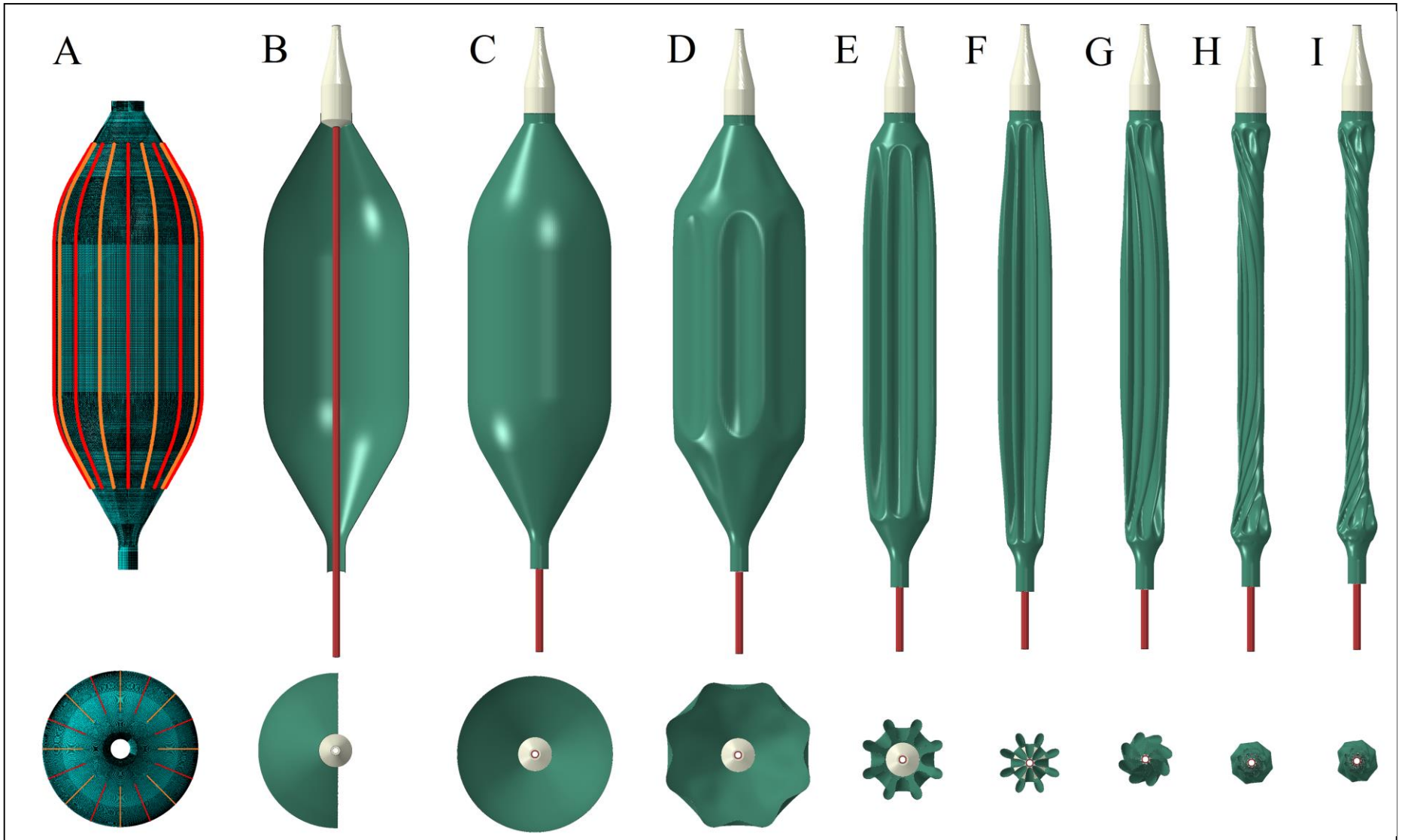

Figure 8. Balloon setup. A: Node sets ‘A’ and ‘B’ are highlighted in red and orange, B-H: The balloon deflating and twisting.

Aortic Root Model

An aortic root model was developed from patient specific MSCT images. The images are of a sixty year old female patient undergoing a coronary angiogram. ScanIP V6 (Simpleware Ltd. 2014) was used to extract the internal volume of the aortic root using thresholding (voxels above 100 hounsfield units were assumed to be in the internal volume), from which the aortic root wall model was derived. The aortic root wall model has a consistent wall thickness of 2.5mm. The native aortic leaflets were modelled separately in ScanIP and were again, based on the MSCT images. The average native aortic leaflet thickness was 1.5mm. Both the aortic root wall and the native leaflets were meshed with ScanIP resulting in 336,562 and 95,024 tetrahedral elements respectively. The aortic root and leaflet models are shown in Figure 9. During the deployment simulation, the native leaflets are attached to the native aortic root wall by means of a tie constraint. The material model used for the aortic root wall and leaflets are summarised in Table 1.

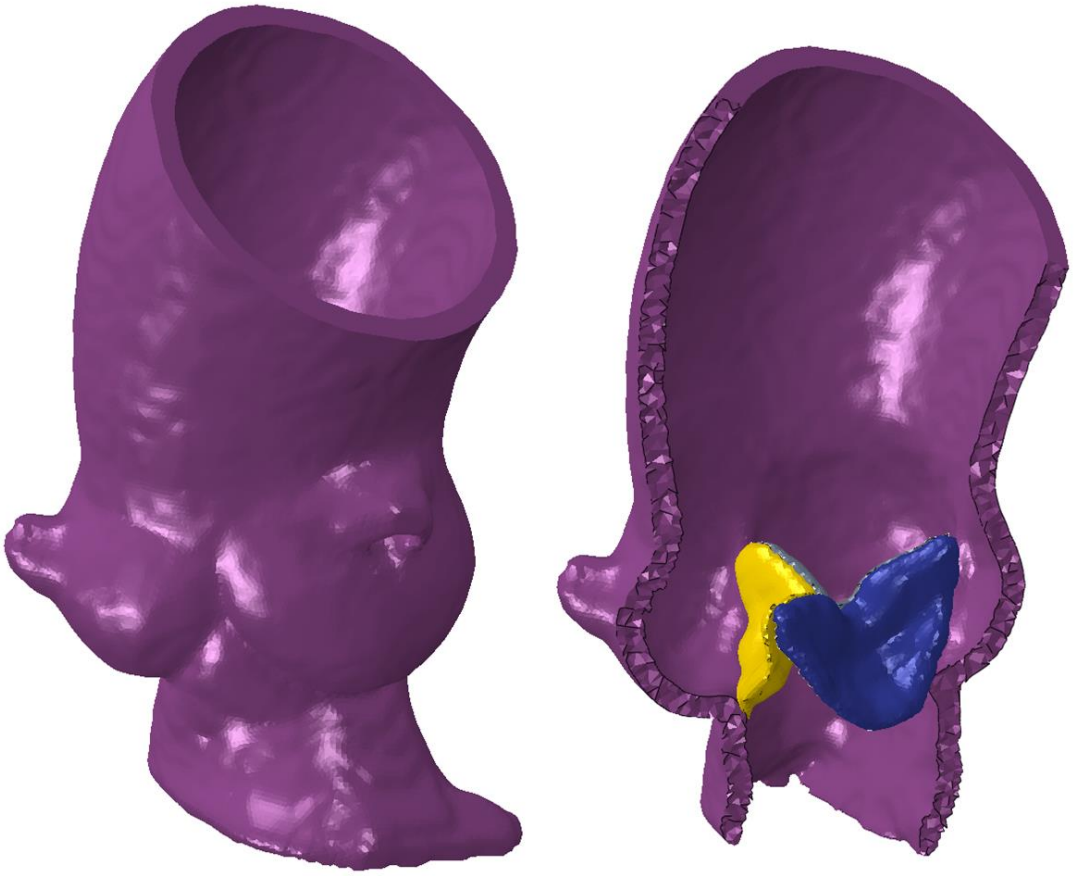

Figure 9. Aortic root model (left) with a section of the aortic root wall removed (right) revealing the native aortic leaflets.

Disclosure Statement

The funding for this project was partially provided by an unrestricted research grant from Medtronic. *[Name removed to maintain the integrity of the review process]* has also received other unrestricted funding from Medtronic, as well as receiving fees for speaking and/or consultancy from Medtronic and St. Jude Medical. *[Name removed to maintain the integrity of the review process]* and *[Name removed to maintain the integrity of the review process]* have no further conflicts of interest to state.